Research Article Vol. 32, No. 3 / 29 Jan 2024 / Optics Express 3804
Optics EXPRESS

Discrepancy of coordinate system selection in backscattering Mueller matrix polarimetry: exploring photon coordinate system transformation invariants

RUI HAO,[1] NAN ZENG,[1] ZHENG ZHANG,[1] HONGHUI HE,[1,3] CHAO HE,[2,4] AND HUI MA[1]

[1]*Guangdong Research Center of Polarization Imaging and Measurement Engineering Technology, Shenzhen Key Laboratory for Minimal Invasive Medical Technologies, Institute of Biopharmaceutical and Health Engineering, Tsinghua Shenzhen International Graduate School, Tsinghua University, Shenzhen 518055, China*
[2]*Department of Engineering Science, University of Oxford, Parks Road, Oxford OX1 3PJ, United Kingdom*
[3]*he.honghui@sz.tsinghua.edu.cn*
[4]*chao.he@eng.ox.ac.uk*

Abstract: In biomedical studies, Mueller matrix polarimetry is gaining increasing attention because it can comprehensively characterize polarization-related vectorial properties of the sample, which are crucial for microstructural identification and evaluation. For backscattering Mueller matrix polarimetry, there are two photon coordinate selection conventions, which can affect the following Mueller matrix parameters calculation and information acquisition quantitatively. In this study, we systematically analyze the influence of photon coordinate system selection on the backscattering Mueller matrix polarimetry. We compare the Mueller matrix elements in the right-handed-nonunitary and non-right-handed-unitary coordinate systems, and specifically deduce the changes of Mueller matrix polar decomposition, Mueller matrix Cloude decomposition and Mueller matrix transformation parameters widely used in backscattering Mueller matrix imaging as the photon coordinate system varied. Based on the theoretical analysis and phantom experiments, we provide a group of photon coordinate system transformation invariants for backscattering Mueller matrix polarimetry. The findings presented in this study give a crucial criterion of parameters selection for backscattering Mueller matrix imaging under different photon coordinate systems.

1. Introduction

As a label-free method to obtain structural and optical information of media, nowadays polarization imaging has been more and more prevalently used in various fields such as remote sensing [1], materials characterization [2], underwater geolocalization [3], and biomedicine [4–6]. Specifically, for biomedical studies and clinical applications, Mueller matrix (MM) imaging is gaining increasing attention because it can comprehensively characterize the sample's polarization-related vectorial properties, which are crucial for microstructural identification and evaluation [7]. Recently, MM microscopy has shown great potential in pathological detection of abnormal tissue areas [8–13]. On the other hand, backscattering MM polarimetry provides a promising tool for quantitative in-vivo and endoscopic tissue measurement [14–19]. To more efficiently acquire the structural and optical information of complex tissue sample contained in a MM, in the past decades several MM analyzing methods have been proposed [20–26]. For instance, the MM polar decomposition (MMPD) decomposes the MM into a product of three matrices, namely diattenuation, retardance and generalized depolarization, to derive a series of polarization feature parameters with clear physical significances [20]. The MM Cloude decomposition

#513999 https://doi.org/10.1364/OE.513999
Journal © 2024 Received 21 Nov 2023; revised 27 Dec 2023; accepted 9 Jan 2024; published 19 Jan 2024

Optics EXPRESS

(MMCD) maps the MM to the Pauli matrix to extract different degrees of depolarization effect [24,25]. Besides, we put forward the Mueller matrix transformation (MMT) based on phantom experiments and Monte Carlo simulations to extract more rotation invariant parameters with clear relationship with certain structures from the MM [26]. All the parameters obtained via MM analyzing methods mentioned above lay the foundation for tissue MM polarimetry.

For backscattering MM polarimetry there are two photon coordinate selection conventions for the light. According to the relationship between the photon coordinate systems of the emergent and incident light, these two conventions are: (i) both the photon coordinate systems of emergent and incident light conform to the right-hand rule. However, their x-axes are not unified, so we call it right-handed-nonunitary (RR) coordinate system (adopted in numerous optics books including Principles of Optics [27] and Light scattering by small particles [28]); (ii) the x-axes of the photon coordinate systems of the emergent and incident light are unified, so we call it non-right-handed-unitary (RL) coordinate system (widely used in tissue polarimetric studies such as Monte Carlo simulation of polarization photons propagation in turbid media [26,29,30]). It should be noted that, here "nonunitary" is used to emphasize that in the RR system, the x-axes of the emergent and incident light are not consistent. "Unitary" is used to emphasize that in the RL system, the x-axes of the emergent and incident light are consistent. Basically, both the conventions are acceptable for backscattering MM imaging. For instance, several experimental and theoretical studies chose the RR coordinate system [31–39], while other researches adopted the RL coordinate system for their measurements [40–48]. However, it should be noted that the following MM parameters calculation and information acquisition are obviously influenced by the photon coordinate selections.

In this study, we analyze the influence of photon coordinate system selection on the backscattering MM polarimetry. We first compare the MM elements in the RR and RL coordinate systems, and specifically deduce the changes of MMPD, MMCD and MMT parameters widely used in backscattering MM imaging as the photon coordinate system varied. Then based on the analysis, a group of photon coordinate system transformation invariants (PCSIs) for backscattering MM polarimetry is provided. The phantom experiments confirm that some MM parameters can be prominently affected by photon coordinate system selection. The effectiveness of the proposed invariant MM parameters is also demonstrated. The findings presented in this study give a crucial criterion of parameters selection for backscattering Mueller matrix imaging under different photon coordinate systems.

2. Mueller matrix elements in different photon coordinate systems

Here, we firstly analyze the influence of different photon coordinate systems on the MM. Figure 1 shows the schematics of two photon coordinates usually used for backscattering polarimetry. Note that for transmission and grazing incidence measurement systems, the emergent light and incident light have the same coordinate as the red arrows show in Fig. 1, where the xyz-axes follow the laboratory coordinate system, and the incident light as the yellow arrow indicated is in the xoz-plane.

Ideally, for a backscattering setup with normal incidence, the incident angle θ is 0 deg; the z-axis of the photon coordinate system is consistent with the incident light wave propagation direction; and the y-axis of the photon coordinate system (the positive direction of the s wave) is consistent with the y-axis of the laboratory coordinate system. As for the real backscattering tissue polarimetry such as MM endoscopy, the incident angle θ is often within 20 deg [49], then the x-axis of the backscattered photon coordinate system (the positive direction of the p wave) can be defined in two ways: (a) approximately opposite to the x-axis of the incident light as Fig. 1(a) shows, where both the emergent light indicated by the blue arrow and the incident light indicated by the yellow arrow conform to the right-hand rule. However, here the x axis of the emergent light is different with that of the incident light. (b) approximately the same as the x-axis of the incident

Optics EXPRESS

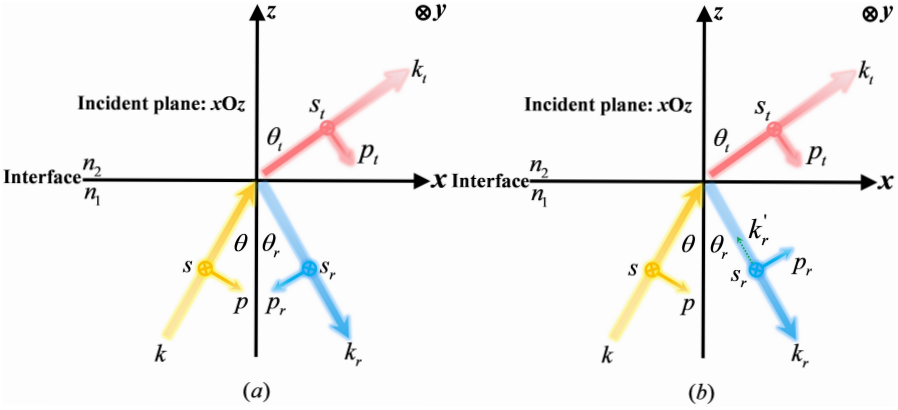

Fig. 1. Schematics of two photon coordinate systems. The incident light is indicated by the yellow arrows, the emergent light is mainly divided into: forward transmitted light indicated by the red arrows and backscattering light indicated by the blue arrows. Their corresponding angles are θ, θ_t and θ_r, respectively. The s wave is indicated by s, the p wave is indicated by p, and the light wave propagation direction is indicated by k. (a) Right-handed-nonunitary (RR) coordinate system. (b) Non-right-handed-unitary (RL) coordinate system. It should be noted that k_r represents the actual light wave propagation direction, and k_r' represents the light wave propagation direction conformed to the right-hand rule.

light as Fig. 1(b) shows, where the emergent light no longer conforms to the right-hand rule, but its x axis definition is mutually unified with that of the incident light. Most optical textbooks, such as Principles of Optics [27] and Light scattering by small particles [28], are discussed in the right-hand rule system illustrated as Fig. 1(a). We call it the right-handed-nonunitary (RR) coordinate system. Meanwhile, for tissue polarimetric studies such as the Monte Carlo simulation of polarization photons propagation in turbid media [26,29,30], the non-right-handed-unitary (RL) coordinate system as shown in Fig. 1(b) were often adopted. Based on the above two coordinate system selections, the MM representations can be derived as shown in Eqs. (1)–(4).

$$\boldsymbol{S}_R^{out} = \boldsymbol{M}_{RR}\boldsymbol{S}_R^{in} \tag{1}$$

$$\boldsymbol{S}_L^{out} = \boldsymbol{M}_{RL}\boldsymbol{S}_R^{in} \tag{2}$$

where $\boldsymbol{S}_R^{in}$ and $\boldsymbol{S}_R^{out}$ represent the Stokes vectors of the incident and emergent light satisfying the right-hand rule, respectively; $\boldsymbol{S}_L^{out}$ represents the Stokes vector of the emergent light satisfying the non-right-hand rule. Accordingly, $\boldsymbol{M}_{RR}$ and $\boldsymbol{M}_{RL}$ are the MM measured in the RR and RL systems, respectively. Note that $\boldsymbol{S}_L^{out}$ can be considered as the symmetry of $\boldsymbol{S}_R^{out}$ with respect to the y axis. Hence, we have the transformation relationship between $\boldsymbol{S}_L^{out}$ and $\boldsymbol{S}_R^{out}$ shown as Eq. (3). Consequently, the relationship between $\boldsymbol{M}_{RR}$ and $\boldsymbol{M}_{RL}$ can be acquired, as shown in Eq. (4).

$$\boldsymbol{S}_L^{out} = diag(1, 1, -1, -1)\boldsymbol{S}_R^{out} \tag{3}$$

Optics EXPRESS

$$\begin{aligned} \boldsymbol{M}_{RL} &= \begin{bmatrix} m_{RL11} & m_{RL12} & m_{RL13} & m_{RL14} \\ m_{RL21} & m_{RL22} & m_{RL23} & m_{RL24} \\ m_{RL31} & m_{RL32} & m_{RL33} & m_{RL34} \\ m_{RL41} & m_{RL42} & m_{RL43} & m_{RL44} \end{bmatrix} \\ &= diag(1,1,-1,-1)\boldsymbol{M}_{RR} = \begin{bmatrix} m_{RR11} & m_{RR12} & m_{RR13} & m_{RR14} \\ m_{RR21} & m_{RR22} & m_{RR23} & m_{RR24} \\ -m_{RR31} & -m_{RR32} & -m_{RR33} & -m_{RR34} \\ -m_{RR41} & -m_{RR42} & -m_{RR43} & -m_{RR44} \end{bmatrix} \end{aligned} \tag{4}$$

According to Eq. (4), apparently the third and fourth rows elements of $\boldsymbol{M}_{RR}$ and $\boldsymbol{M}_{RL}$ have opposite signs, which can further affect the calculation and analysis of the MM derived parameters measured using backscattering polarimetry. Thus, to explore the influence of the RR and RL photon coordinate systems selection on backscattering MM derived parameters images, in the following sections we take Eqs. (1)–(4) as the basis for the derivation and demonstration of the three groups of MM derived parameters frequently used in tissue polarimetry, namely MMPD, MMCD and MMT.

3. Mueller matrix polar decomposition method

As one of the most prevalently used analyzing tools in tissue polarimetry, the MMPD method [20] assumes that the optical behavior in a biomedical sample is continuous and follows the order of dichroism (D), retardance (R), and generalized depolarization (Δ), as indicated by Eq. (5).

$$\begin{aligned} \boldsymbol{M} &= \left(m_{ij}\right)_{4\times4} = m_{11}\left(M_{ij}\right)_{4\times4} = \boldsymbol{M}_{\Delta}\boldsymbol{M}_{R}\boldsymbol{M}_{D} \\ &= m_{11}\begin{bmatrix} 1 & \vec{\boldsymbol{D}}^{T} \\ \vec{\boldsymbol{P}} & \boldsymbol{m}_{3\times3} \end{bmatrix} = \begin{bmatrix} 1 & \vec{\boldsymbol{0}}^{T} \\ \vec{\boldsymbol{P}}_{\Delta} & \boldsymbol{m}_{\Delta} \end{bmatrix}\begin{bmatrix} 1 & \vec{\boldsymbol{0}}^{T} \\ \vec{\boldsymbol{0}} & \boldsymbol{m}_{R} \end{bmatrix}\begin{bmatrix} 1 & \vec{\boldsymbol{D}}^{T} \\ \vec{\boldsymbol{D}} & \boldsymbol{m}_{D} \end{bmatrix} \end{aligned} \tag{5}$$

In Eq. (5), m_{ij} represents the unnormalized MM element, and M_{ij} represents the MM element normalized by m_{11}. Here, i and j denote the corresponding row and column indices of the MM element, respectively. Based on Eq. (5), the dichroism vector $\vec{\boldsymbol{D}}$ and its modulus D can be calculated directly by using the first row elements of $\boldsymbol{M}$, as shown in Eq. (6) and (7).

$$\vec{\boldsymbol{D}} = \left[M_{12}, M_{13}, M_{14}\right]^{T} \tag{6}$$

$$D = \sqrt{{M_{12}}^2 + {M_{13}}^2 + {M_{14}}^2} = \frac{1}{m_{11}}\sqrt{{m_{12}}^2 + {m_{13}}^2 + {m_{14}}^2} \tag{7}$$

On the basis of Eq. (6) and (7), we can further obtain the dichroism matrix $\boldsymbol{M}_D$ and its lower-right 3×3 submatrix $\boldsymbol{m}_D$, as shown in Eq. (8) and Eq. (9).

$$\boldsymbol{M}_{D} = \begin{bmatrix} 1 & \vec{\boldsymbol{D}}^{T} \\ \vec{\boldsymbol{D}} & \boldsymbol{m}_{D} \end{bmatrix} \tag{8}$$

$$\boldsymbol{m}_{D} = \sqrt{1-D^2}\boldsymbol{I} + \left(1-\sqrt{1-D^2}\right)\vec{\boldsymbol{D}}\vec{\boldsymbol{D}}^{T} \tag{9}$$

According to Eqs. (6)–(9), since $\vec{\boldsymbol{D}}$, D, $\boldsymbol{M}_D$ and $\boldsymbol{m}_D$ can all be calculated directly from the first row elements of $\boldsymbol{M}$ without involving the elements from third and fourth rows, the RR and

Optics EXPRESS

RL photon coordinate systems selection does not affect the dichroism parameters, which are all PCSIs.

Next, we can separate the dichroism matrix $\boldsymbol{M}_D$ from $\boldsymbol{M}$ to get the product matrix $\boldsymbol{M}'$ of the generalized depolarization matrix $\boldsymbol{M}_\Delta$ and the retardance matrix $\boldsymbol{M}_R$ and its lower-right 3×3 submatrix $\boldsymbol{m}'$, as shown in Eq. (10). Further, the generalized depolarization matrix $\boldsymbol{M}_\Delta$ and its lower-right 3×3 submatrix $\boldsymbol{m}_\Delta$ can be constructed as shown in Eqs. (11) and (12). Finally, the scalar parameter Δ used to characterize the depolarization effect can be obtained by calculating the rank of $\boldsymbol{m}_\Delta$, as shown in Eq. (13). Here, $\vec{\boldsymbol{P}}_\Delta$ denotes the polarizance vector and $\mathrm{eig}\,(\cdot)$ denotes the eigenvalue of the matrix.

$$\boldsymbol{M}' = \boldsymbol{M}\boldsymbol{M}_D^{-1} = \boldsymbol{M}_\Delta \boldsymbol{M}_R = \begin{bmatrix} 1 & \vec{\boldsymbol{0}}^T \\ \vec{\boldsymbol{P}}_\Delta & \boldsymbol{m}_\Delta \end{bmatrix} \begin{bmatrix} 1 & \vec{\boldsymbol{0}}^T \\ \vec{\boldsymbol{0}} & \boldsymbol{m}_R \end{bmatrix} = \begin{bmatrix} 1 & \vec{\boldsymbol{0}}^T \\ \vec{\boldsymbol{P}}_\Delta & \boldsymbol{m}_\Delta \boldsymbol{m}_R \end{bmatrix} = \begin{bmatrix} 1 & \vec{\boldsymbol{0}}^T \\ \vec{\boldsymbol{P}}_\Delta & \boldsymbol{m}' \end{bmatrix} \tag{10}$$

$$\boldsymbol{M}_\Delta = \begin{bmatrix} 1 & \vec{\boldsymbol{0}}^T \\ \vec{\boldsymbol{P}}_\Delta & \boldsymbol{m}_\Delta \end{bmatrix} \tag{11}$$

$$\begin{aligned} &\boldsymbol{m}_\Delta = \pm\left(\boldsymbol{m}_\Delta^a\right)^{-1} \boldsymbol{m}_\Delta^b \\ &\boldsymbol{m}_\Delta^c = \boldsymbol{m}' \left(\boldsymbol{m}'\right)^T \\ &\mathrm{eig}\left(\boldsymbol{m}_\Delta^c\right) = \lambda_i, i = 1, 2, 3 \\ &\boldsymbol{m}_\Delta^a = \boldsymbol{m}_\Delta^c + \left(\sqrt{\lambda_1\lambda_2} + \sqrt{\lambda_1\lambda_3} + \sqrt{\lambda_2\lambda_3}\right) \boldsymbol{I}_{3\times3} \\ &\boldsymbol{m}_\Delta^b = \left(\sqrt{\lambda_1} + \sqrt{\lambda_2} + \sqrt{\lambda_3}\right) \boldsymbol{m}_\Delta^c + \sqrt{\lambda_1\lambda_2\lambda_3} \boldsymbol{I}_{3\times3} \end{aligned} \tag{12}$$

$$\Delta = 1 - \frac{|\mathrm{tr}\,(\boldsymbol{m}_\Delta)|}{3} = 1 - \frac{|\mathrm{tr}(\boldsymbol{M}_\Delta) - 1|}{3} \tag{13}$$

As $\boldsymbol{M}_D$ is a PCSI, combined with Eq. (10), we can deduce that $\boldsymbol{M}'$, $\boldsymbol{m}'$ and $\vec{\boldsymbol{P}}_\Delta$ satisfy the following relations in the RR and RL coordinate systems:

$$\boldsymbol{M}'_{RL} = diag(1, 1, -1, -1)\boldsymbol{M}'_{RR} \tag{14}$$

$$\vec{\boldsymbol{P}}_{\Delta RL} = diag(1, -1, -1)\vec{\boldsymbol{P}}_{\Delta RR} \tag{15}$$

$$\boldsymbol{m}'_{RL} = diag(1, -1, -1)\boldsymbol{m}'_{RR} \tag{16}$$

Substituting Eq. (16) into Eq. (12), it can be observed that $\boldsymbol{m}^c_{\Delta RR}$ and $\boldsymbol{m}^c_{\Delta RL}$ exhibit a "Fish-shaped" relationship, which are symmetric matrices in common but the elements along their upper edge, left edge, upper-right corner, and lower-left corner, have opposite signs. Here, we denote this "Fish-shaped" transformation operation as $Fish\,(\cdot)$, as indicated in Eqs. (17) and (18). Because that the determinant expansions of the two matrices satisfying the "Fish-shaped" relationship are the same with respect to their eigenvalues, it means the eigenvalues of $\boldsymbol{m}^c_{\Delta RR}$ and

Optics EXPRESS

$\boldsymbol{m}^c_{\Delta RL}$ are equal, as shown in Eq. (19).

$$\boldsymbol{m}^c_{\Delta RR} = \begin{bmatrix} m^c_{\Delta RR11} & m^c_{\Delta RR12} & m^c_{\Delta RR13} \\ m^c_{\Delta RR12} & m^c_{\Delta RR22} & m^c_{\Delta RR23} \\ m^c_{\Delta RR13} & m^c_{\Delta RR23} & m^c_{\Delta RR33} \end{bmatrix} \tag{17}$$

$$\boldsymbol{m}^c_{\Delta RL} = Fish\left(\boldsymbol{m}^c_{\Delta RR}\right) = \begin{bmatrix} m^c_{\Delta RR11} & -m^c_{\Delta RR12} & -m^c_{\Delta RR13} \\ -m^c_{\Delta RR12} & m^c_{\Delta RR22} & m^c_{\Delta RR23} \\ -m^c_{\Delta RR13} & m^c_{\Delta RR23} & m^c_{\Delta RR33} \end{bmatrix} \tag{18}$$

$$\mathrm{eig}\left(\boldsymbol{m}^c_{\Delta RR}\right) = \mathrm{eig}\left(\boldsymbol{m}^c_{\Delta RL}\right) \tag{19}$$

Based on Eqs. (12) and (19), since the "Fish-shaped" $\boldsymbol{m}^c_{\Delta RR}$ and $\boldsymbol{m}^c_{\Delta RL}$ have the equal eigenvalues, $\boldsymbol{m}^a_{\Delta}$ and $\boldsymbol{m}^b_{\Delta}$ also exhibit a similar "Fish-shaped" relationship in the RR and RL coordinate systems. Then, by substituting Eqs. (17) and (18) into Eq. (12) and taking the inverse of $\boldsymbol{m}^a_{\Delta RR}$ and $\boldsymbol{m}^a_{\Delta RL}$, we can derive the following relationship:

$$\begin{aligned} \left(\boldsymbol{m}^a_{\Delta RR}\right)^{-1} &= \frac{1}{\left|\boldsymbol{m}^a_{\Delta RR}\right|}\left(\boldsymbol{m}^a_{\Delta RR}\right)^* \\ \left(\boldsymbol{m}^a_{\Delta RL}\right)^{-1} &= \frac{1}{\left|\boldsymbol{m}^a_{\Delta RL}\right|}\left(\boldsymbol{m}^a_{\Delta RL}\right)^* = \frac{1}{\left|\boldsymbol{m}^a_{\Delta RR}\right|} Fish\left[\left(\boldsymbol{m}^a_{\Delta RR}\right)^*\right] \\ \left(\boldsymbol{m}^a_{\Delta RL}\right)^{-1} &= Fish\left[\left(\boldsymbol{m}^a_{\Delta RR}\right)^{-1}\right] \end{aligned} \tag{20}$$

Considering that the determinants of $\boldsymbol{m}^a_{\Delta RR}$ and $\boldsymbol{m}^a_{\Delta RL}$ are equal, and the adjoint matrices of $\boldsymbol{m}^a_{\Delta RR}$ and $\boldsymbol{m}^a_{\Delta RL}$ satisfy the "Fish-shaped" relationship, it can be concluded that the inverse matrices of $\boldsymbol{m}^a_{\Delta RR}$ and $\boldsymbol{m}^a_{\Delta RL}$ also maintain the "Fish-shaped" relationship. In other words, the process of taking inverses does not change the "Fish-shaped" relationship. To ultimately obtain the depolarization parameter Δ, Eq. (20) should be substituted into Eq. (12), to obtain the specific expressions of $\boldsymbol{m}_{\Delta}$ in both RR and RL coordinate systems:

$$\begin{aligned} \boldsymbol{m}_{\Delta RR} &= \pm\left(\boldsymbol{m}^a_{\Delta RR}\right)^{-1}\boldsymbol{m}^b_{\Delta RR} \\ \boldsymbol{m}_{\Delta RL} &= \pm\left(\boldsymbol{m}^a_{\Delta RL}\right)^{-1}\boldsymbol{m}^b_{\Delta RL} = \pm Fish\left[\left(\boldsymbol{m}^a_{\Delta RR}\right)^{-1}\right] Fish\left(\boldsymbol{m}^b_{\Delta RR}\right) = \pm Fish(\boldsymbol{m}_{\Delta RR}) \end{aligned} \tag{21}$$

From Eq. (21), it can be observed that $\boldsymbol{m}_{\Delta}$ satisfies the "Fish-shaped" relationship in both photon coordinate systems. Similar to Eq. (19), the eigenvalues of $\boldsymbol{m}_{\Delta RR}$ and $\boldsymbol{m}_{\Delta RL}$ are equal. Therefore, we can conclude that the depolarization parameter Δ is a PCSI, as shown in Eq. (22).

$$\begin{aligned} \Delta_{RR} &= 1 - \frac{\left|\mathrm{tr}\left(\boldsymbol{m}_{\Delta RR}\right)\right|}{3} = 1 - \frac{\left|\sum \mathrm{eig}\left(\boldsymbol{m}_{\Delta RR}\right)\right|}{3} \\ \Delta_{RL} &= 1 - \frac{\left|\mathrm{tr}\left(\boldsymbol{m}_{\Delta RL}\right)\right|}{3} = 1 - \frac{\left|\sum \mathrm{eig}\left(\boldsymbol{m}_{\Delta RL}\right)\right|}{3} \\ \Delta_{RL} &= \Delta_{RR} \end{aligned} \tag{22}$$

With this, we can separate the retardance matrix $\boldsymbol{M}_R$ from $\boldsymbol{M}'$ and proceed the discussion of linear retardance, optical rotation, and other polarization parameters, as shown in Eqs. (23)–(27).

$$\boldsymbol{M}_R = \begin{bmatrix} 1 & \vec{\boldsymbol{0}}^T \\ \vec{\boldsymbol{0}} & \boldsymbol{m}_R \end{bmatrix} \tag{23}$$

Optics EXPRESS

$$\boldsymbol{m}_R = (\boldsymbol{m}_\Delta)^{-1}\boldsymbol{m}' \tag{24}$$

$$R = \arccos\left(\frac{\mathrm{tr}\,(\boldsymbol{M}_R)}{2} - 1\right) \tag{25}$$

$$\delta = \arccos\sqrt{(M_{R22} + M_{R33})^2 + (M_{R32} - M_{R23})^2} - 1 \tag{26}$$

$$\alpha = \frac{1}{2}\arctan\left(\frac{M_{R32} - M_{R23}}{M_{R22} + M_{R33}}\right) \tag{27}$$

where $\boldsymbol{m}_R$ represents the lower-right 3×3 submatrix of retardance matrix $\boldsymbol{M}_R$, R is the overall retardance, δ represents the linear retardance, and α represents the optical rotation. As demonstrated in Eq. (20), the matrix inverse operation does not change the "Fish-shaped" relationship. Therefore, combining it with Eqs. (16) and (24), we have the following relationship:

$$\boldsymbol{M}_{RRL} = diag(1, 1, -1, -1)\boldsymbol{M}_{RRR} \tag{28}$$

It is evident from Eq. (28) that the elements in the third and fourth rows of $\boldsymbol{M}_R$ have the opposite signs in RR and RL coordinate systems. Therefore, the parameters R, δ, α computed from Eqs. (25)–(27) relying on the photon coordinate system are all photon coordinate system transformation variants.

4. Mueller matrix Cloude decomposition method

The MMCD method [24,25] is another widely used tool in MM tissue polarimetry. The general steps of a MMCD decomposition are as follows:

Firstly, the MM is mapped to a Hermite matrix $\boldsymbol{H}(\boldsymbol{M})$ using the Pauli matrix $\boldsymbol{\sigma}$ as the basis, as shown in Eq. (29).

$$\begin{aligned} &\boldsymbol{H}(\boldsymbol{M}) = \frac{1}{4}\sum_{i,j=1}^{4} m_{ij}\boldsymbol{\sigma}_i \otimes \boldsymbol{\sigma}_j \\ &\boldsymbol{\sigma}_1 = \begin{bmatrix} 1 & 0 \\ 0 & 1 \end{bmatrix}, \boldsymbol{\sigma}_2 = \begin{bmatrix} 1 & 0 \\ 0 & -1 \end{bmatrix}, \boldsymbol{\sigma}_3 = \begin{bmatrix} 0 & 1 \\ 1 & 0 \end{bmatrix}, \boldsymbol{\sigma}_4 = \begin{bmatrix} 0 & i \\ -i & 0 \end{bmatrix} \end{aligned} \tag{29}$$

Then, the four real eigenvalues of $\boldsymbol{H}(\boldsymbol{M})$ are arranged in descending order as $\lambda_1 \geq \lambda_2 \geq \lambda_3 \geq \lambda_4 \geq 0$, which contains crucial information related to depolarization. When the depolarization exists, the eigenvalues are non-zero, and we can establish the following relationship:

$$\boldsymbol{H}(\boldsymbol{M}) = \frac{1}{m_{11}}\sum_{i=1}^{4}\lambda_i\boldsymbol{H}_i \tag{30}$$

where $\boldsymbol{H}_i$ represents the non-zero eigenvalue λ_i corresponding to the matrix obtained by the outer product of the eigen vector. Moreover, $\boldsymbol{H}_i$ has a rank of 1. Hence, Eq. (30) essentially decomposes the MM into the sum of at most four nondepolarizing matrices. By substituting Eq. (4) into Eq. (30), the specific forms of $\boldsymbol{H}(\boldsymbol{M})$ in both RR and RL coordinate systems can be

Optics EXPRESS

derived, as shown in Eq. (31) and (32).

$$\boldsymbol{H}(\boldsymbol{M})_{RR} = \begin{bmatrix} h_{11} & h_{12} & h_{13} & h_{14} \\ \overline{h}_{12} & h_{22} & h_{23} & h_{24} \\ \overline{h}_{13} & \overline{h}_{23} & h_{33} & h_{34} \\ \overline{h}_{14} & \overline{h}_{24} & \overline{h}_{34} & h_{44} \end{bmatrix} \tag{31}$$

$$\boldsymbol{H}(\boldsymbol{M})_{RL} = \begin{bmatrix} h_{11} & h_{12} & -h_{13} & -h_{14} \\ \overline{h}_{12} & h_{22} & -h_{23} & -h_{24} \\ -\overline{h}_{13} & -\overline{h}_{23} & h_{33} & h_{34} \\ -\overline{h}_{14} & -\overline{h}_{24} & \overline{h}_{34} & h_{44} \end{bmatrix} \tag{32}$$

As a series of MMCD parameters are all related to the eigenvalues of $\boldsymbol{H}(\boldsymbol{M})$, we can compute the eigenvalues of $\boldsymbol{H}(\boldsymbol{M})_{RR}$ and $\boldsymbol{H}(\boldsymbol{M})_{RL}$, which confirm that their determinants have the same expansion, thus satisfying the relationship of equal eigenvalues:

$$\mathrm{eig}\left[\boldsymbol{H}(\boldsymbol{M})_{RR}\right] = \mathrm{eig}\left[\boldsymbol{H}(\boldsymbol{M})_{RL}\right] \tag{33}$$

Several studies have performed combination operations on the eigenvalues of $\boldsymbol{H}(\boldsymbol{M})$, thereby obtaining parameters such as polarization entropy [50,51], indices of polarimetric purity [52,53], depolarization index [54], and overall purity index [55], as shown in Eqs. (34)–(37).

$$S(\boldsymbol{H}) = -\sum_{i=1}^{4}\left(\frac{\lambda_i}{m_{11}}\log_4\left(\frac{\lambda_i}{m_{11}}\right)\right) \tag{34}$$

$$\begin{aligned} P_1 &= \frac{\lambda_1 - \lambda_2}{m_{11}} \\ P_2 &= \frac{\lambda_1 + \lambda_2 - 2\lambda_3}{m_{11}} \\ P_3 &= \frac{\lambda_1 + \lambda_2 + \lambda_3 - 3\lambda_4}{m_{11}} \end{aligned} \tag{35}$$

$$P_\Delta = \sqrt{\frac{1}{3}\left(2P_1^2 + \frac{2}{3}P_2^2 + \frac{1}{3}P_3^2\right)} \tag{36}$$

$$PI = \sqrt{\frac{1}{3}\left(P_1^2 + P_2^2 + P_3^2\right)} \tag{37}$$

Apparently, since the calculations of MMCD parameters above only involve the eigenvalue λ and matrix element m_{11}, which do not depend on the photon coordinate system selection, it can be concluded that the MMCD parameters are all PCSIs.

5. Mueller matrix transformation method

The MMT method [26] mainly focuses on directly mapping polarization parameters with clear physical significance through combination operations on MM elements, offering high computational efficiency for in vivo tissue MM polarimetry. Here in this section, we discuss and

Optics EXPRESS

analyze the frequently used MMT parameters in backscattering MM imaging, as presented in Eqs. (38)–(43).

$$\|\boldsymbol{B}\| = {M_{22}}^2 + {M_{33}}^2 + {M_{23}}^2 + {M_{32}}^2 \tag{38}$$

$$b = \frac{M_{22} + M_{33}}{2} \tag{39}$$

$$t_2 = \sqrt{M_{12}^2 + M_{13}^2} \tag{40}$$

$$t_3 = \sqrt{M_{42}^2 + M_{43}^2} \tag{41}$$

$$x_2 = \frac{1}{2}\arctan\left(\frac{M_{31}}{M_{21}}\right) \tag{42}$$

$$A = \frac{2t_1 b}{{t_1}^2 + b^2} = \frac{2 \cdot \frac{\sqrt{(M_{22}-M_{33})^2+(M_{23}+M_{32})^2}}{2} \cdot \frac{M_{22}+M_{33}}{2}}{\frac{(M_{22}-M_{33})^2+(M_{23}+M_{32})^2}{4} + \left(\frac{M_{22}+M_{33}}{2}\right)^2} \tag{43}$$

where $\|\boldsymbol{B}\|$ represents the second norm of the central block of the MM, whose value is related to retardance and dichroism; $1 - b$ is used to characterize the depolarization effect; t_2 represents dichroism; t_3 is used to characterize retardance; x_2 shows the direction of dichroism; and A represents the degree of overall anisotropy of the media. As the MMT parameters are explicitly expressed in terms of the MM elements, it is straightforward to determine their responses to the RR and RL coordinate system transformation according to Eq. (4). For instance, the parameter t_2 shown in Eq. (40) is obviously a PCSI, as it is directly derived from the M_{12} and M_{13}. As for the parameters $\|\boldsymbol{B}\|$ and t_3, their expressions shown in Eqs. (38) and (41) contain squared calculations, which effectively eliminate the impact of the photon coordinate system transformation on the M_{32}, M_{33}, M_{42} and M_{43}, rendering them all PCSIs. However, for the parameters b and A shown as Eqs. (39) and (43), their calculations involve the third row of MM, thus depending on the choice of RR or RL coordinate system. It is worth noting that the proof approach for other MMT parameters is similar as discussed above.

In summary, we have successfully derived and demonstrated the PCSIs of MMPD, MMCD, and MMT, as presented in Table 1.

Table 1. Photon coordinate system transformation invariants in the Mueller matrix derived parameters. (*T* indicates the invariant and *F* indicates the variant under the photon coordinate system transformation)

MMPD	D	Δ	R	δ	α	θ
	T	T	F	F	F	F
MMCD	$S(\boldsymbol{H})$	P_1	P_2	P_3	P_Δ	PI
	T	T	T	T	T	T
MMT	$\|\boldsymbol{B}\|$	b	t_2	t_3	x_2	A
	T	F	T	T	F	F

6. Experimental results and analysis

To further validate the influence of the RR and RL coordinate systems selection on the MM derived parameters, we experimentally measured the MM of an anisotropic phantom composed of concentrically well aligned silks, whose effectiveness for revealing the relationship between fibrous structures and backscattering polarimetric parameters has been demonstrated previously [26,43]. The experimental results of several MM derived parameters are illustrated in Fig. 2.

Optics EXPRESS

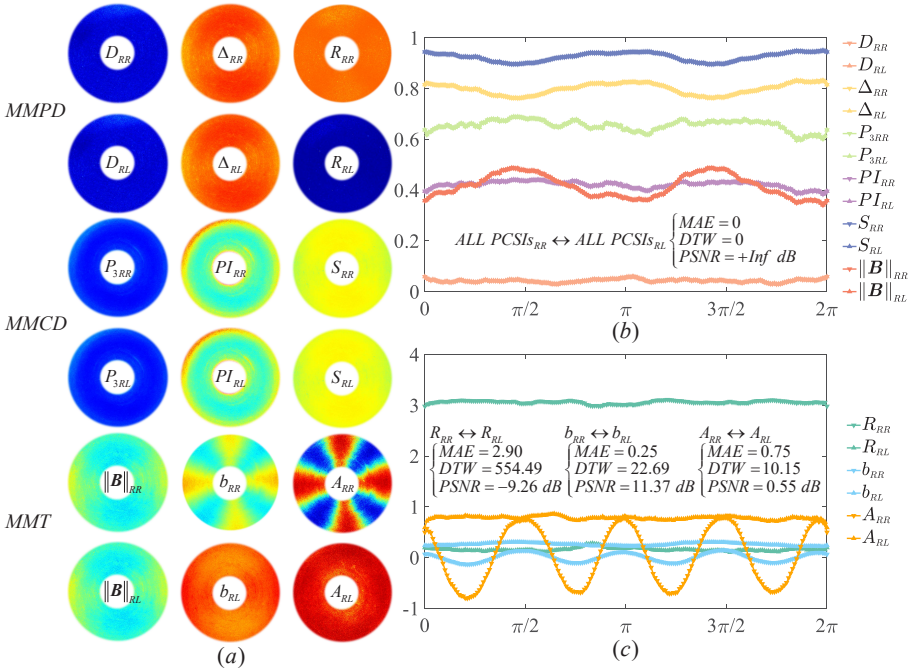

Fig. 2. (a) Experimental results of MM derived parameters for the silk phantom. For each class of MM derived parameters, the upper row and lower row represent the measurement results under RR and RL coordinate systems, respectively. (b) Azimuthal curves of photon coordinate system transformation invariants (the units of P_3 and PI are 1×10^3). (c) Azimuthal curves of the photon coordinate system transformation variants. Additionally, in (b) and (c), the horizontal and vertical axes represent the azimuth angle and parameter value, respectively.

We can observe from Fig. 2(a) that for the PCSIs D, Δ, P_3, PI, S ($\boldsymbol{H}$) and $\|\boldsymbol{B}\|$, the measurement results under RR (upper row) and RL (lower row) coordinate systems are the same. However, the variants R, b and A images exhibit prominent differences between the RR and RL coordinate systems. Especially, the periodical intensity variations of MMT parameters b and A are apparently errors induced by coordinate transformation. To more clearly compare the measurement results in Fig. 2(a), we obtain the azimuthal curves for each parameter within the range of $[0, 2\pi]$ as shown in Fig. 2(b) and (c). Furthermore, the differences between the parameters in the two coordinate systems are quantitatively evaluated by using indicators of mean absolute error (MAE), dynamic time warping (DTW) and peak signal-to-noise ratio (PSNR). For the PCSIs as shown in Fig. 2(b), the MAE, DTW, and PSNR values in both coordinate systems exhibit ideal values. When it comes to the variant parameter R, its azimuthal curves exhibit the most significant difference between the two coordinate systems, with each indicator also deviating the most from the ideal values. For the variants b and A, their curves display characteristics of rotation invariant [56] in the RL system. However, in the RR system, their curves show periodical intensity variations of false negative values within the range of $[0, 2\pi]$, which contradicts their true physical significance. It is evident that for backscattering MM polarimetry such as MM endoscopy, the choice of photon coordinate system is crucial to acquire correct MM derived parameters analyzing results.

Optics EXPRESS

7. Conclusions

In this study, we analyzed the influence of photon coordinate system selection on the backscattering MM polarimetry. We first compared the MM elements in the RR and RL coordinate systems. It showed that the third and fourth rows elements of $\boldsymbol{M}_{RR}$ and $\boldsymbol{M}_{RL}$ have opposite signs, which can further affect the calculation and analysis of the MM derived parameters measured using backscattering polarimetry. Then we specifically deduced the changes of MMPD, MMCD and MMT parameters widely used in backscattering MM imaging as the photon coordinate system varied. Based on the analysis, we provided a group of photon coordinate system transformation invariants for backscattering MM polarimetry as MMPD parameters D and Δ, MMT parameters $\|\boldsymbol{B}\|$, t_2 and t_3, and all MMCD parameters. The phantom experiments further confirmed that some MM parameters can be prominently influenced by photon coordinate system selection. The effectiveness of the proposed invariant MM parameters was also demonstrated by evaluation indicators as MAE, DTW, and PSNR. Evidently, for backscattering MM polarimetry such as MM endoscopy, the choice of photon coordinate system should be clarified to acquire correct MM derived parameters analyzing results. The findings presented in this study give a crucial criterion of parameters selection for backscattering Mueller matrix imaging under different photon coordinate systems.

Funding. Shenzhen Key Fundamental Research Project (No. JCYJ20210324120012035).

Acknowledgements. Chao He would like to thank the support of the Junior Research Fellowship from St John's College, University of Oxford.

Disclosures. The authors declare that there are no conflicts of interest related to this article.

Data availability. Data underlying the results presented in this paper are not publicly available at this time but maybe obtained from the authors upon reasonable request.

References

1. J. S. Tyo, D. L. Goldstein, D. B. Chenault, *et al.*, "Review of passive imaging polarimetry for remote sensing applications," Appl. Opt. **45**(22), 5453–5469 (2006).
2. S. Liu, W. Du, X. Chen, *et al.*, "Mueller matrix imaging ellipsometry for nanostructure metrology," Opt. Express **23**(13), 17316–17329 (2015).
3. X. Bai, Z. Liang, Z. Zhu, *et al.*, "Polarization-based underwater geolocalization with deep learning," eLight **3**(1), 15 (2023).
4. C. He, H. He, J. Chang, *et al.*, "Polarisation optics for biomedical and clinical applications: a review," Light: Sci. Appl. **10**(1), 194 (2021).
5. H. He, R. Liao, N. Zeng, *et al.*, "Mueller matrix polarimetry-an emerging new tool for characterizing the microstructural feature of complex biological specimen," J. Lightwave Technol. **37**(11), 2534–2548 (2018).
6. J. Qi and D. S. Elson, "Mueller polarimetric imaging for surgical and diagnostic applications: a review," J. Biophotonics **10**(8), 950–982 (2017).
7. C. He, J. Chang, P. S. Salter, *et al.*, "Revealing complex optical phenomena through vectorial metrics," Adv. Photonics **4**(02), 026001 (2022).
8. M. Zaffar and A. Pradhan, "Assessment of anisotropy of collagen structures through spatial frequencies of mueller matrix images for cervical pre-cancer detection," Appl. Opt. **59**(4), 1237–1248 (2020).
9. Y. Dong, J. Wan, L. Si, *et al.*, "Deriving polarimetry feature parameters to characterize microstructural features in histological sections of breast tissues," IEEE Trans. Biomed. Eng. **68**(3), 881–892 (2020).
10. T. Liu, M. Lu, B. Chen, *et al.*, "Distinguishing structural features between crohn's disease and gastrointestinal luminal tuberculosis using mueller matrix derived parameters," J. Biophotonics **12**(12), e201900151 (2019).
11. Y. Dong, J. Qi, H. He, *et al.*, "Quantitatively characterizing the microstructural features of breast ductal carcinoma tissues in different progression stages by mueller matrix microscope," Biomed. Opt. Express **8**(8), 3643–3655 (2017).
12. M. Dubreuil, P. Babilotte, L. Martin, *et al.*, "Mueller matrix polarimetry for improved liver fibrosis diagnosis," Opt. Lett. **37**(6), 1061–1063 (2012).
13. Y. Shen, R. Huang, H. He, *et al.*, "Comparative study of the influence of imaging resolution on linear retardance parameters derived from the mueller matrix," Biomed. Opt. Express **12**(1), 211–225 (2021).
14. J. Qi, T. Tatla, E. Nissanka-Jayasuriya, *et al.*, "Surgical polarimetric endoscopy for the detection of laryngeal cancer," Nat. Biomed. Eng. **7**(8), 971–985 (2023).
15. C. Buckley, M. Fabert, D. Kinet, *et al.*, "Design of an endomicroscope including a resonant fiber-based microprobe dedicated to endoscopic polarimetric imaging for medical diagnosis," Biomed. Opt. Express **11**(12), 7032–7052 (2020).

Optics EXPRESS

16. M. Gataric, G. S. Gordon, F. Renna, *et al.*, "Reconstruction of optical vector-fields with applications in endoscopic imaging," IEEE Trans. Med. Imaging **38**(4), 955–967 (2018).
17. Y. Fu, Z. Huang, H. He, *et al.*, "Flexible 3×3 mueller matrix endoscope prototype for cancer detection," IEEE Trans. Instrum. Meas. **67**(7), 1700–1712 (2018).
18. S. Manhas, J. Vizet, S. Deby, *et al.*, "Demonstration of full 4×4 mueller polarimetry through an optical fiber for endoscopic applications," Opt. Express **23**(3), 3047–3054 (2015).
19. S. Rivet, A. Bradu, and A. Podoleanu, "70 khz full 4x4 mueller polarimeter and simultaneous fiber calibration for endoscopic applications," Opt. Express **23**(18), 23768–23786 (2015).
20. S.-Y. Lu and R. A. Chipman, "Interpretation of mueller matrices based on polar decomposition," J. Opt. Soc. Am. A **13**(5), 1106–1113 (1996).
21. R. Ossikovski, "Differential matrix formalism for depolarizing anisotropic media," Opt. Lett. **36**(12), 2330–2332 (2011).
22. N. Ortega-Quijano and J. L. Arce-Diego, "Mueller matrix differential decomposition," Opt. Lett. **36**(10), 1942–1944 (2011).
23. N. Ortega-Quijano and J. L. Arce-Diego, "Depolarizing differential mueller matrices," Opt. Lett. **36**(13), 2429–2431 (2011).
24. S. R. Cloude, "Group theory and polarisation algebra," Optik (Stuttgart) **75**, 26–36 (1986).
25. S. R. Cloude, "Conditions for the physical realisability of matrix operators in polarimetry," in *Polarization Considerations for Optical Systems II*, vol. 1166 (SPIE, 1990), pp. 177–187.
26. H. He, N. Zeng, E. Du, *et al.*, "A possible quantitative mueller matrix transformation technique for anisotropic scattering media/eine mögliche quantitative müller-matrix-transformations-technik für anisotrope streuende medien," Photonics Lasers Med. **2**(2), 129–137 (2013).
27. M. Born and E. Wolf, *Principles of optics: electromagnetic theory of propagation, interference and diffraction of light* (Elsevier, 2013).
28. H. C. Hulst and H. C. van de Hulst, *Light scattering by small particles* (Courier Corporation, 1981).
29. J. C. Ramella-Roman, S. A. Prahl, and S. L. Jacques, "Three monte carlo programs of polarized light transport into scattering media: part i," Opt. Express **13**(12), 4420–4438 (2005).
30. T. Yun, N. Zeng, W. Li, *et al.*, "Monte carlo simulation of polarized photon scattering in anisotropic media," Opt. Express **17**(19), 16590–16602 (2009).
31. Z. Wang and H. Gao, "Accounting for light source angular distribution in backscattering mueller matrix interpretation using double-planar small-angle scattering trajectory approximation," Journal of Quantitative Spectroscopy and Radiative Transfer **278**, 108030 (2022).
32. Y. Deng, S. Zeng, Q. Lu, *et al.*, "Characterization of backscattering mueller matrix patterns of highly scattering media with triple scattering assumption," Opt. Express **15**(15), 9672–9680 (2007).
33. S. Badieyan, A. Dilmaghani-Marand, M. J. Hajipour, *et al.*, "Detection and discrimination of bacterial colonies with mueller matrix imaging," Sci. Rep. **8**(1), 10815 (2018).
34. B. D. Cameron, Y. Li, and A. Nezhuvingal, "Determination of optical scattering properties in turbid media using mueller matrix imaging," J. Biomed. Opt. **11**(5), 054031 (2006).
35. M. Hornung, A. Jain, M. Frenz, *et al.*, "Interpretation of backscattering polarimetric images recorded from multiply scattering systems: a study on colloidal suspensions," Opt. Express **27**(5), 6210–6239 (2019).
36. S. Badieyan, A. Ameri, M. R. Razzaghi, *et al.*, "Mueller matrix imaging of prostate bulk tissues; polarization parameters as a discriminating benchmark," Photodiagn. Photodyn. Ther. **26**, 90–96 (2019).
37. H. Wang, H. Hu, J. Jiang, *et al.*, "Polarization differential imaging in turbid water via mueller matrix and illumination modulation," Opt. Commun. **499**, 127274 (2021).
38. Y.-R. Liu, C.-F. Liang, H.-Q. Zhao, *et al.*, "A polarization image enhancement method for glioma," Front. Neurosci. **17**, 1163701 (2023).
39. I. Berezhnyy and A. Dogariu, "Time-resolved mueller matrix imaging polarimetry," Opt. Express **12**(19), 4635–4649 (2004).
40. M. Sun, H. He, N. Zeng, *et al.*, "Characterizing the microstructures of biological tissues using mueller matrix and transformed polarization parameters," Biomed. Opt. Express **5**(12), 4223–4234 (2014).
41. T. Liu, T. Sun, H. He, *et al.*, "Comparative study of the imaging contrasts of mueller matrix derived parameters between transmission and backscattering polarimetry," Biomed. Opt. Express **9**(9), 4413–4428 (2018).
42. T.-V. Nguyen, T.-H. Nguyen, N. B.-T. Nguyen, *et al.*, "Evaluation of optical features of fibronectin fibrils by backscattering polarization imaging," Optik **272**, 170304 (2023).
43. H. He, M. Sun, N. Zeng, *et al.*, "Mapping local orientation of aligned fibrous scatterers for cancerous tissues using backscattering mueller matrix imaging," J. Biomed. Opt. **19**(10), 106007 (2014).
44. S. Manhas, M. K. Swami, P. Buddhiwant, *et al.*, "Mueller matrix approach for determination of optical rotation in chiral turbid media in backscattering geometry," Opt. Express **14**(1), 190–202 (2006).
45. H.-M. Le, T. H. Le, Q. H. Phan, *et al.*, "Mueller matrix imaging polarimetry technique for dengue fever detection," Opt. Commun. **502**, 127420 (2022).
46. M. Sun, H. He, N. Zeng, *et al.*, "Probing microstructural information of anisotropic scattering media using rotation-independent polarization parameters," Appl. Opt. **53**(14), 2949–2955 (2014).

Optics EXPRESS

47. C. He, H. He, X. Li, *et al.*, "Quantitatively differentiating microstructures of tissues by frequency distributions of mueller matrix images," J. Biomed. Opt. **20**(10), 105009 (2015).
48. M.-R. Antonelli, A. Pierangelo, T. Novikova, *et al.*, "Impact of model parameters on monte carlo simulations of backscattering mueller matrix images of colon tissue," Biomed. Opt. Express **2**(7), 1836–1851 (2011).
49. Z. Zhang, C. Shao, H. He, *et al.*, "Analyzing the influence of oblique incidence on quantitative backscattering tissue polarimetry: a pilot ex vivo study," J. Biomed. Opt. **28**(10), 102905 (2023).
50. R. Barakat, "Polarization entropy transfer and relative polarization entropy," Opt. Commun. **123**(4-6), 443–448 (1996).
51. C. Brosseau, *Fundamentals of polarized light: a statistical optics approach*, (Wiley-Interscience, New York, 1998).
52. J. J. Gil, "Polarimetric characterization of light and media: physical quantities involved in polarimetric phenomena," Eur. Phys. J. Appl. Phys. **40**(1), 1–47 (2007).
53. I. San José and J. J. Gil, "Invariant indices of polarimetric purity: generalized indices of purity for n× n covariance matrices," Opt. Commun. **284**(1), 38–47 (2011).
54. J. J. Gil and E. Bernabeu, "A depolarization criterion in mueller matrices," Opt. Acta **32**(3), 259–261 (1985).
55. A. Tariq, P. Li, D. Chen, *et al.*, "Physically realizable space for the purity-depolarization plane for polarized light scattering media," Phys. Rev. Lett. **119**(3), 033202 (2017).
56. P. Li, D. Lv, H. He, *et al.*, "Separating azimuthal orientation dependence in polarization measurements of anisotropic media," Opt. Express **26**(4), 3791–3800 (2018).